

# We are IntechOpen, the world's leading publisher of Open Access books Built by scientists, for scientists

6,900

Open access books available

185,000

International authors and editors

200M

Downloads

Our authors are among the

154

Countries delivered to

TOP 1%

most cited scientists

12.2%

Contributors from top 500 universities



WEB OF SCIENCE™

Selection of our books indexed in the Book Citation Index  
in Web of Science™ Core Collection (BKCI)

Interested in publishing with us?  
Contact [book.department@intechopen.com](mailto:book.department@intechopen.com)

Numbers displayed above are based on latest data collected.  
For more information visit [www.intechopen.com](http://www.intechopen.com)



# Hybrid Liquid-Crystal/Photonic-Crystal Devices: Current Research and Applications

*Yu-Cheng Hsiao*

## Abstract

In this chapter, the current research and development of the liquid crystal-based photonic crystals is introduced. This chapter will present the essential knowledge of the new photonic crystal technology and applications in simple language. In the recent year, liquid crystal-enabled photonic crystal technologies have attracted broad attentions from scientists. Based on special optical properties of liquid crystal-enabled photonic crystal device, many applications, such as tunable optical filters, tunable optical modulators, optical pulse compressors, laser device, and applications in multiphoton microscopy, have been developed in recent years. In addition, the detailed optical properties, operation principles, and prospects are discussed in this chapter.

**Keywords:** photonic crystals, liquid crystals, photonic band gap, electro-optic device, optical properties

## 1. Introduction

### 1.1 Liquid crystal-based photonic crystal devices

Photonic crystals (PCs) are structural materials with periodically varying dielectric permittivity. The term PC was coined three decades ago, and fascinating properties of PCs have attracted numerous scientists to put in a great deal of effort. PCs consist of dielectric materials. In PCs, the index of refraction varies periodically in space. PCs were invented since 1987, when both Yablonovitch and John published their results independently [1, 2]. The most important characteristic of PCs is the photonic band gap (PBG). Furthermore, the PBG of PCs is an optical analog to the electronic bandgap in semiconductor materials, which means photons will be localized or forbidden in the PCs. Based on this characteristic, PCs can be used as various photonic applications [3–7]. However, if a defect layer is introduced to a PC structure, disrupting its periodicity, the transmission of photons at specific wavelengths will be induced within the PBG; these narrow transmission bands within PBG are called defect modes. Based on this special design of PCs with defect layers, many photonic device applications were proposed: PC lasers [8], PC optical fibers [9], and other optical devices [10, 11]. In addition, the spectral properties of the PCs can be controlled if the defect layer is tunable, for instance, liquid crystal (LC).

LCs are anisotropic materials. The optic axis (or molecular orientation) can be controlled by applying electric field, magnetic field, or temperature. Based on optical anisotropy, LC can be used as a phase retarder or an optical polarization rotator, of which the refractive indices can be tuned with external fields. LCs are also used in many other applications such as displays, smart windows, and optical fibers. Furthermore, by inserting a LC layer as a defect layer in PCs, the tunable defect modes can be achieved. The first tunable LC-based PC hybrid structure was developed by Ozaki et al. They employed a planar-aligned nematic LC as a central defect layer sandwiched between two one-dimensional (1D) PCs [12]. **Figure 1** shows the setup of the designed hybrid PC/LC cell. This idea was then extended to PC/cholesteric LC (CLC) structures for tunable laser applications [13–17]. CLCs are self-organized PCs, in which the molecular chirality forms helical structures with the optic axis continuously twisted along the helical axis. The effects of angle of incidence [18], temperature [19], and magnetic field [20] on the optical properties of PC/LC devices are investigated.

Zyryanov et al. investigated the hybrid PC/LC device between the crossed polarizers. Their experimental results show attractive features of the tunable defect modes within the PBG. The wavelengths of defect modes are shifted by the change in effective refractive index ( $n_{\text{eff}}$ ) [21]. Larger number of defect modes can be induced by using high refractive index LC or by increasing the thickness of the LC defect layer. Moreover, they experimentally and theoretically demonstrated that the interference of defect modes can be achieved by placing the cell between crossed polarizers. The orthogonal polarization components through vector sum in the projection direction along the axis of the analyzer lead to shift of defect modes. As a result, the transmittance is increased when the defect mode wavelength of an extraordinary component overlaps that of an ordinary one in PCs [20].

In addition, the next milestone is electrically tunable photonic device based on PC/CLC and PC/polymer-stabilized CLC (PSCLC) hybrid structures [22–24]. With the PC/PSCLC structure, not only the wavelength of defect mode is switchable among multistable states by voltage pulses, but also the optical intensity of defect modes can be electrically tuned through switching among different metastable states. **Figure 2** shows the sandwiched structure of the PC/PSCLCs in the three stable states. It is wavelength switchable and intensity tunable of defect modes among three stable states. The unique optical tristability in the defect modes reduces power consumption and enhances flexibility. From then on, the PC and CLC combined

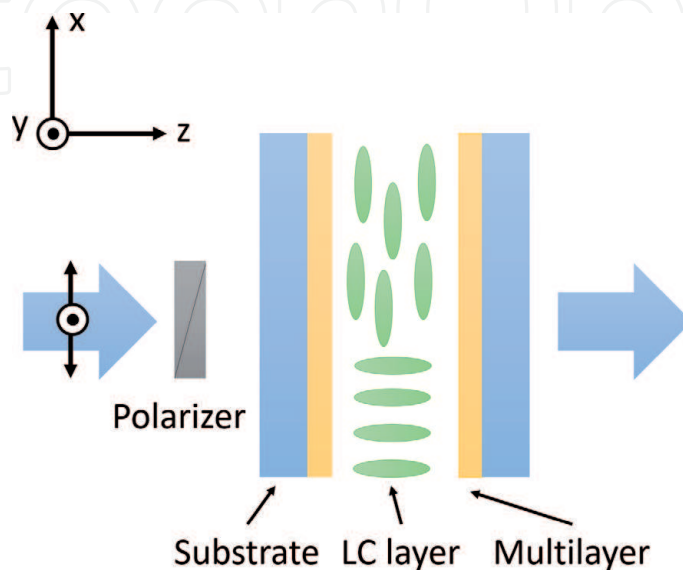


**Figure 1.**  
*Schematic of the PC/LC hybrid device in an electro-optical setup.*

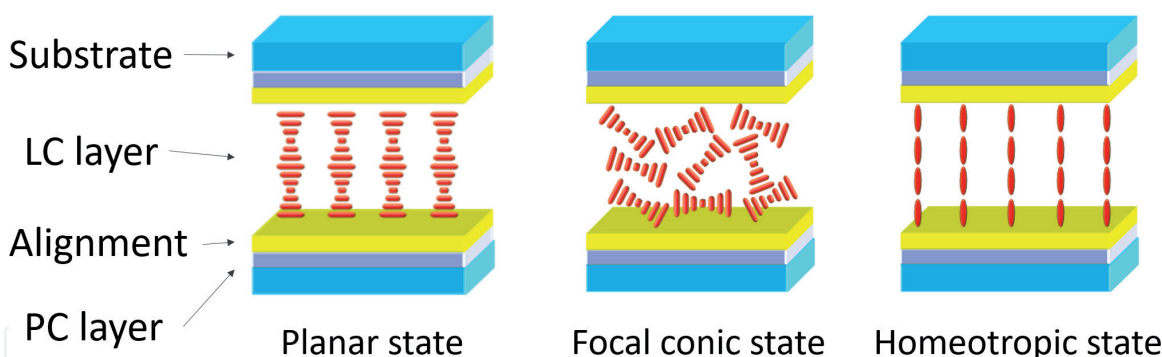


**Figure 2.**  
 Schematic of the PC/CLC hybrid device in three stable states.

devices became a hot topic. Many types of PC/chiral LC hybrid devices are invented such as PC/BHN, PC/THN, and PC/PSCT. Recently, many scientists employ hybrid PC/CLC to achieve the lasing applications [25, 26].

## 1.2 Aim of this chapter

An overview of the development of PC/LC is presented. The optical properties, operation principles, and applications of liquid crystal-based photonic crystal devices are discussed. In Section 1, I introduce the basic knowledge of LC and PC physics to make the reader understand the next section. Section 2 details the operation principles of nonchiral and chiral LC modes to help the understanding of switching mechanisms described in two following sections. In addition, the optical properties of defect modes in different LC states are reported in Section 2. Section 2.1 is “Photonic crystals with a nonchiral nematic liquid crystal,” Section 2.2 is “Chiral-tilted homeotropic nematic liquid crystal-based photonic crystal devices,” Section 2.3 is “Chiral nematic and cholesteric liquid crystal with photonic crystal devices,” and Section 2.4 is “Tristable photonic crystal devices with polymer-stabilized cholesteric textures.” The configuration of many types of PC/LC cell applications, including the design of PC multilayers for applications is schematically depicted in Session 3. To realize the PC applications; Session 3.1 introduces “Electrically switchable liquid crystal-based photonic crystals for a white light laser,” Session 3.2 shows “Liquid crystal-based photonic crystals for pulse compression and signal enhancement in fluorescence applications,” and Session 3.3 demonstrates “Photo-manipulated photonic devices based on tristable chiral-tilted homeotropic nematic liquid crystal.” Finally, I will summarize the results and conclude about this chapter.

## 2. Operation method of liquid crystal-based photonic crystal devices

### 2.1 Photonic crystals with a nonchiral nematic liquid crystal

Nowadays, available LC materials can be classified into two categories: non-chiral and chiral system, according to their different operation functions on their molecule arrangement. The nonchiral LC owns only one stable arrangement state, which is determined by the use of the alignment layer. In addition, nonchiral LC molecule is continuously oriented, when the voltage is applied. On the contrary, two or multistable states are exhibited in the chiral LC system. Moreover, the multistable states can be switched and controlled from one to another based on the condition of applied voltage pulse. Based on the properties of the nonchiral LC system, it can serve as a phase retarder or optical rotator tuned by electrically



controlled birefringence (ECB) effect. Combined with the PC cells from Prof. Ozaki introduced in Section 1.1, the LC defect layers used are nonchiral LCs, and it can be operated like phase retarders. In order to understand the PC/nonchiral LC, operation method of PC/LC devices is most important. The operation method of the PC/LC in nonchiral type as tunable defect can be described in terms of two effects: ordinary and extraordinary refractive indices effects [12, 20, 27]. From **Figure 1** in Section 1.1, the positive dielectric anisotropy of the nonchiral LC is aligned along the x-axis as well as the light propagates along the z-axis. In addition, the PC structure consists of two dielectric materials: high and low refractive index materials, which are stacked alternatively. When the light is incident to the hybrid PC/LC device normally as well as the light polarization direction parallel to the LC molecule along the x-axis, the extraordinary refractive index ( $n_e$ ) contributed the optical path length (OPL) is exhibited. Thus, the appearance of defect modes in the PBG represents extraordinary defect modes. When the electric field is applied across the PC/LC device to make LC molecule along the z-axis, the OPL is only contributed by the sole ordinary refractive index ( $n_o$ ). The sole  $n_o$  makes the OPL decreasing, and the ordinary defect modes shift to the shorter wavelength. However, the wavelength of defect modes in PBG remains unchanged, when the field-on and field-off are applied, because the polarization direction of the incoming light is in the y-axis and the same  $n_o$  contribution of the OPL is unchanged. We can conclude that the tunability of the defect modes is attributed to the change in refractive index ( $n_e$  or  $n_o$ ) and its corresponding OPL.

In addition, the other nonchiral type is the twisted-nematic (TN) LC, in which the molecular orientation only exhibits  $90^\circ$  twist, acts like the optical polarization rotator, so that the incoming light passing through the TN LC is characterized by the rotation of polarization. The hybrid PC/TN LC structure was first demonstrated in 2010 [28]. The optical phenomena attributable to the PC/TN LC structure are quite different from the mechanism mentioned in the preceding paragraph. The  $90^\circ$  TN LC modes are divided into three groups based on the polarization angle  $\beta$  between the axis of the first polarizer and the director axis lying in the front substrate. They are classified as the ordinary-mode (O-mode), extraordinary-mode (E-mode), and mixed-mode (M-mode), and then TN satisfies the conditions of  $\beta = 90, 0$ , and  $45^\circ$ , respectively. The M-mode TN (abbreviated as MTN) combines both the polarization-rotation effect and birefringence effect. **Figure 3** shows the phenomenon of the wavelength shift of defect modes in two PC/TN cells impregnated with two different nematic LC materials. The defect modes of PC/TN for the ordinary ray are independent of the applied electric field. However, the wavelengths of defect modes in PBG with both E-mode and O-mode in PC/TN device are also shown as the blueshift, when we increase the applied voltage. This effect is unlike the ECB-based defect modes of PC/LC in the preceding paragraph. Compared with the O-mode and the E-mode in PC/TN, ECB-based PC exhibits more blueshift in wavelength because of the decrease in effective refractive index of defect layer significantly. This PC/TN result can be explained by Mauguin parameters [29]. A perfect adiabatic following in the TN LC makes the linearly polarized light to traverse the LC with the rotation of the LC molecular twist, makes the effective refractive index with the incident light nearly equal to  $n_e$  in E-mode and  $n_o$  in O-mode. The  $n_{\text{eff}}$  is no longer a constant in the O-mode TN LC cell, but becomes a weak dependence with applied voltage. Thus, the small shifts for the defect modes are demonstrated in the O-mode PC/TN cells. The most important is the integrated effect (M-mode) of defect modes in PC/TN device. The wavelengths of defect peaks in the M-mode are located at the same wavelength positions of the E-mode and O-mode because the defect peaks of the M-mode in PC/TN are contributed by two effects: the adiabatic following and birefringence effects of LC. Moreover, the intensity of the transmittance of

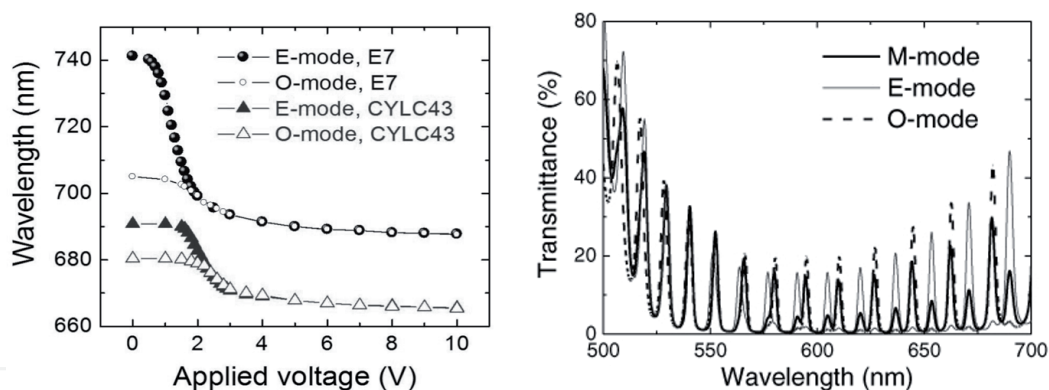


**Figure 3.** The blueshift of defect modes for both E- and O-modes in PC/TN system, and transmittance of the PC/TN in the photonic bandgap with three different modes (adapted from [28]).

defect mode in E- or O-mode spreads to the other, making the intensity of the transmittance of the defect modes in the M-mode almost the same as both in E- or O-mode. Thus, we can observe that the M-mode is a superposition of both E-mode and O-mode. In addition, we observe carefully the spectra of E- and O-mode, small defect peaks accompanying the main defect modes are observed. This phenomenon is very different comparing with other types of PC/LC cells. Finally, no matter PC/LC or PC/TN, the PC-based nonchiral LC is the useful tool for optical devices or photonic applications.

## 2.2 Chiral-tilted homeotropic nematic liquid crystal-based photonic crystal devices

We introduce one of the chiral-type LC called bistable homeotropic nematic LC (BHN). Recently, the green energy concept is concerned with not only how to generate clean energy, but also how to save energy. Following this trend, PC devices with low energy consumption are highly desired. The novel device: a PC infiltrated with a BHN to achieve both the tunability of defect modes and the low energy consumption. The BHN bistable switching mechanisms involve the backflow and the frequency revertible dielectric anisotropy effect [30]. The PC/BHN can perform in two stable states, the tilted homeotropic (tH) and tilted twist (tT) states with nonvoltage. In addition, the two voltage-sustained states: the biased homeotropic (bH) and biased twist (bT) states at frequency 1 and 100 kHz, respectively, are proposed. **Figure 4** shows the LC configurations of the PC/BHN device in both tH state and tT state at 0 V; bH state and bT state at 10 V and 1 kHz. In addition, the switching between the bistable tH and tT states can be achieved by applying short voltage pulses to permit the BHN to pass through the intermediate states (bH and bT) [30]. In this BHN, the voltage-sustained states are necessary pathways for bistable operation served as the transient states. However, no voltage has to be applied to sustain the bistable tH and tT states, making PC device with green energy. The spectra of defect modes in the PC/BHN are interesting. The four states (tT, tH, bT, and bH) have different spectral profiles. The bH state at 10 V<sub>rms</sub> exhibits the defect modes attributed to the ordinary refractive index, all the other states tT, tH, and bT have more peaks spectra caused by the effective refractive index. In addition, the intensity of the extraordinary defect modes in the tH state can be tuned by switching between the tH and bH states as intensity modulator. In the condition, the defect modes will diminish when the stable tH state transforms to the bH state at high voltages. This finding makes PC/BHN device with light-on and light-off states without any polarizers. In addition, **Figure 5** demonstrates the experimental spectra

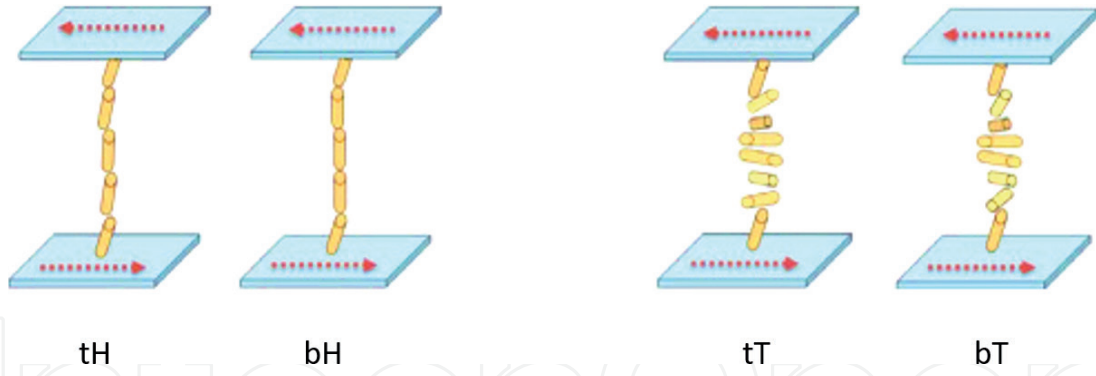


**Figure 4.** LC configurations of the PC/BHN device. The tH state and tT state are at 0 V; bH and bT state are at 10 V and 1 kHz (adapted from [30]).

of a PC/BHN cell in the four bH, tH, bT, and tT states under the parallel polarizer. We can observe that the different spectra of bH, tH, bT, and tT are shown under the parallel polarizer.

Therefore, the PC/BHN device placed between a pair of linear polarizers has been proposed recently [30], and the axes of the two polarizers were parallel or perpendicular to each other in the new PC/BHN system. **Figure 5** demonstrates the bH state exhibited the defect modes corresponding to the sole ordinary refractive index  $n_o$ . From **Figure 5**, we can see that the defect modes of the bH state did not change with  $\phi$  because of the LC molecules oriented vertically. In addition, the stable tT state was obtained from the bT state by turning off the high applied frequency. Comparing with the bT state, the tT state possessed a higher tilt angle, implying that the birefringence effect became more significant. Thus, both the ordinary and extraordinary components were conspicuous. Moreover, from **Figure 5**, the complementary in terms of defect mode wavelengths between the conditions of  $\phi = 0$  and  $90^\circ$  in the tT state was clearly shown. Furthermore, **Figure 6** shows the simulated spectra for the two tH and bH states under the parallel polarizer scheme with various polarization angles. We can observe that the differently distributed defect modes are shown. The calculation of the optical responses for both the bH and tH states by the transfer matrix method is also proposed [30]. The perfect agreement is satisfied between the simulated spectra and the experimental data (**Figure 6**). The profile width at half-maximum (FWHM) of the simulated defect mode peaks is narrower than the experimental one. This is attributable to minor experimental uncertainties like interface roughness and imperfect dielectric materials. Based on tunable optical properties of defect modes in PC/BHN, many photonic applications can be achieved.

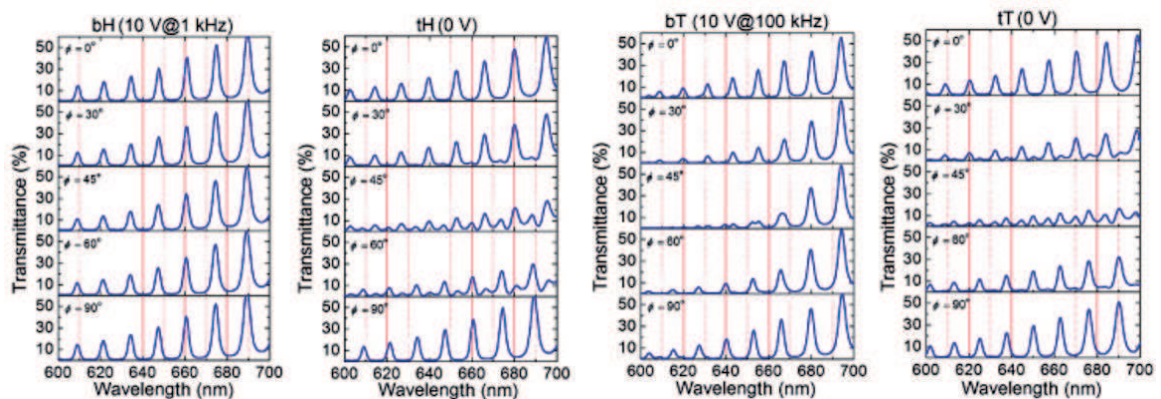


**Figure 5.** Transmission spectra within the PBG of a PC/BHN device in four different states (bH, tH, bT, and tT) (adapted from [30]).



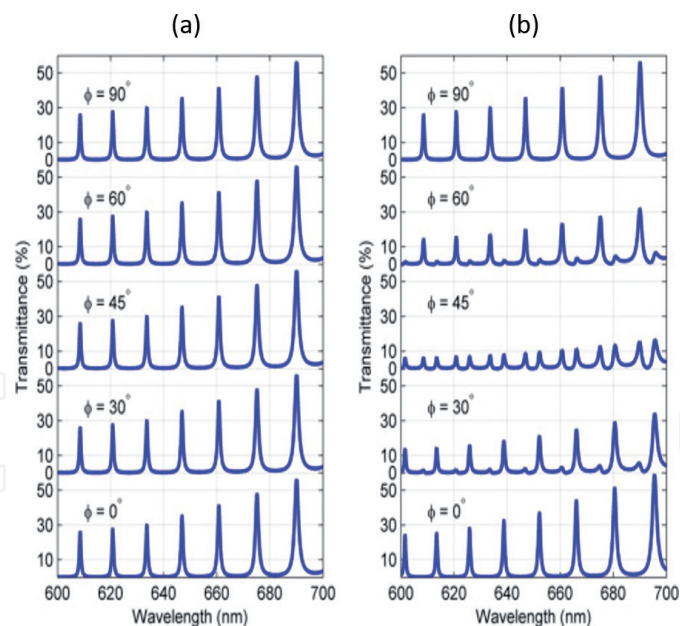


**Figure 6.**  
 Simulations of the transmission spectra of a PC/BHN device under the parallel polarizer at various polarization angles in (a) bH and (b) tH states (adapted from [30]).

In conclusion, a novel photonic structure PC/BHN with stopband, defect mode tunability and optical bistability have been shown. The BHN as a defect layer infiltrated within a PC was investigated recently. With the rich optical properties in the PC/BHN system and its association with the polarization effect, PC/BHN device further opens up new possible applications for the low-power consumption photonic devices in tunable spectral bandwidth and optical multichannel technologies.

### 2.3 Chiral nematic and cholesteric liquid crystal with photonic crystal devices

Comparing with the nematic LCs, the configuration of a cholesteric LC (CLC) or chiral LC with stacked layers shows a periodic helix of LC molecule. CLC characterized by a specific pitch length makes the structure regarded as 1D PC material by itself. The optical Bragg reflection or photonic band is the most important property in CLCs. Utilizing the special properties of periodic helix-induced photonic band in CLCs, many optic applications such as low-threshold single-mode laser with band edge excitation has been proposed. In addition, the special type of CLC is a dual frequency CLC (DFCLC). And DFCLC owns many special properties such as fast switching. Typical CLCs own bistable states, namely, the planar (P) and focal conic (FC) states. And then CLCs cannot directly switch from the FC state to the P state. Typically, this transition must be passing through an intermediate state: homeotropic (H) state or the transient P state [22–24]. However, the DFCLCs made of a DF nematic LC mixed with a chiral dopant could achieve fast and direct FC-to-P switching ( $\sim 10$  ms) [30]. In DFCLC, the dielectric anisotropy is positive and the LC director tends to be paralleled to the electrical field direction (tend to H state) when applied frequency below the crossover frequency. In contrast, the dielectric anisotropy is negative when the applying frequency is higher than the crossover frequency. And the DFCLC director tends to be vertical to the field direction (tend to FC and P states). Therefore, we can use frequency-modulated voltage to switch between the bistable P and FC states reversibly, making the PC/CLC device with more tunable and switchable properties. Based on PC/CLC device, many applications such as intensity tunable and fast switching in the defect mode PC device. The detail structure of the PC/CLC device has been depicted in **Figure 7**. In addition,



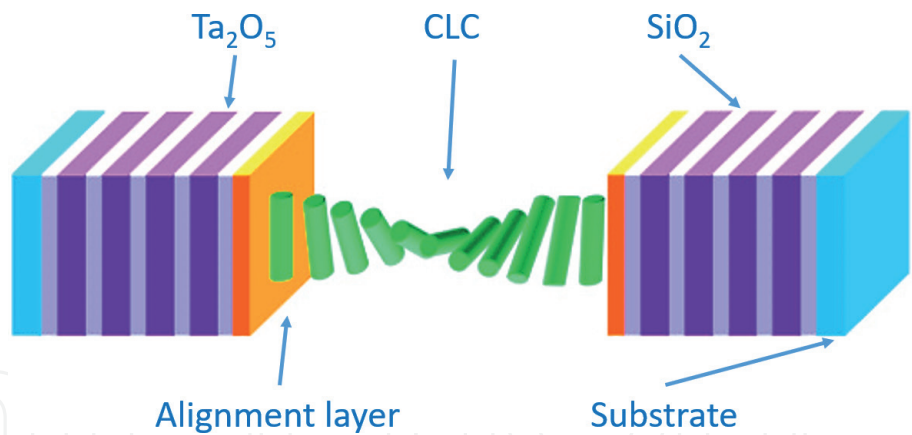


**Figure 7.**  
The sandwich structure of the 1D PC/DFCLC device (adapted from [22–24]).

**Figure 8** shows the transmission spectra of the PC/DFCLC device in three distinctive states (P, FC, and H states) at a various voltages. Among the three states, the P and FC states are optical stable states except the H state. Moreover, the stable P state can be achieved from the unstable H state by fast turning off the applied voltage or from the stable FC state by applying high frequency pulse [22–24]. In addition, **Figure 8** also shows that the hybrid PC/CLC device in the P state, which demonstrates a number of defect modes. Furthermore, the FC state of the hybrid PC device is exhibited when we apply voltage pulse of  $20 V_{rms}$ . The optical intensity of the defect modes is very low in the FC state, and the spectra of defect modes in FC are shown in **Figure 8**. The light scattering properties of FC state make all defect modes turn off. This optical effect has the potential to expand as a fast switching light shutter application. Furthermore, the PC/CLC device will be in the H state when the voltage increases to  $35 V_{rms}$ . And the most intense defect modes of H state are generated. **Figure 8** also shows the comparison of the spectra of defect modes between the P and H states in the PC/CLC device. We can observe that the blueshift of the defect modes of H state is shown and caused by the reduced effective index of refraction in the PC defect layer. It is interesting to observe the special phenomenon “complementary” in wavelengths of defect modes. This property can make the PC/CLC device as a tunable shutter in specific wavelengths of defect modes.

The interesting optical characteristics of PC/CLC devices have been investigated. By using the electrically controllable DFCLC materials as defect layer in the

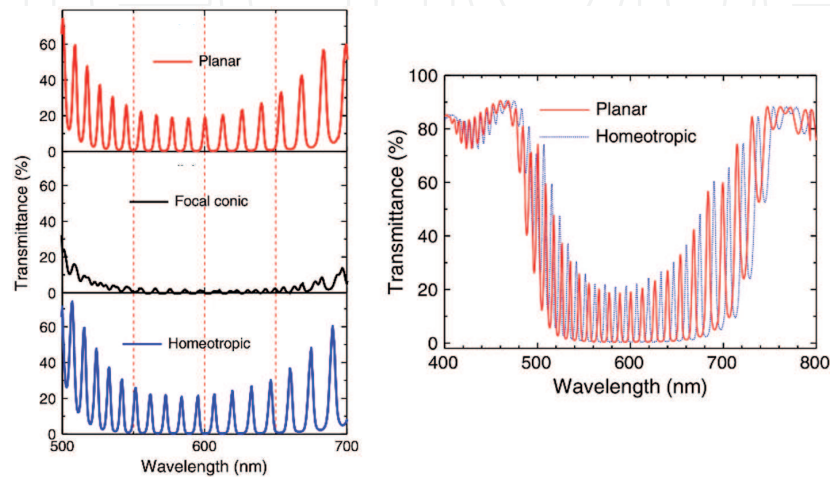


**Figure 8.**  
Spectra of the PC/DFCLC device in the photonic bandgap in P, FC, and H states. The PC/DFCLC device is driven by various voltages. In addition, the PC/DFCLC in the photonic bandgap with two different sets of defect modes in both P and H states (adapted from [22–24]).

PC structure, PC/CLC device owns more powerful properties. Based on the three distinctive states of the CLC defect layer (stable P and FC states, and the voltage-sustained H state), the PC/CLC device exhibits different spectra in different LC states. In addition, the strength and wavelengths of the defect modes can be tuned by applying voltage and frequency. Moreover, the novel PC/CLC device is characterized by its fast switching between P and FC states. In the past research, the FC-to-P transition time is as short as 10 ms [22–24]. The wavelength and intensity tunability in the defect modes are more obvious comparing with other PC device. In addition, it requires no polarizers and is of low-power consumption because of bistability in P and FC states. This PC/CLC device is useful tool for photonic applications such as filter, light shutter, and optical modulator.

2.4 Tristable photonic crystal devices with polymer-stabilized cholesteric textures

In comparison with the typical CLC materials, with inclusion of a photo-polymerizable monomer into CLCs, which make CLC more powerful. The CLC/monomer composites own polymer networks to stabilize the CLC molecule, and we call the composite material as polymer-stabilized cholesteric texture (PSCT). The PSCTs can be employed in green energy devices due to the new stable state in the polymer-stabilized H state. This allows the bistable switching between the FC and P states in CLC become tristable P, FC, and H states potentially [22–24]. In the past, bistable PSCT shutters can also be switched between the H and FC states [31]. However, PSCTs are possible to own more than two stable modes. Recently, Hsiao et al. proposed the first tristable PSCT as a new PC device. **Figure 9** shows three photographs of P, FC, and H states and the corresponding micrographs of the PC/PSCT devices. In addition, the PC/PSCT is placed between two crossed polarizers in the tristable P, FC, and H states. We can discover that the colors are distinctive in the three different stable states. Firstly, the P state shows that the purple color due to the transmittance of defect modes are higher in red wavelength range. In addition, the light scattering FC state shows the multidomains of the PSCT and is presented in **Figure 9**. Moreover, the stable H state with the light leakage under crossed polarizers is also demonstrated in **Figure 9**. In addition, **Figure 10** demonstrates the spectra of defect modes in PC/PSCT device in three distinctive states (P, FC, and H states) at null voltage. The number of defect modes will increase with the increasing defect layer thickness [22–24]. Haiso et al. apply a fixed voltage ( $50\text{ V}_{\text{rms}}$ ) at various frequencies to show the tristable states in PC/PSCT. From **Figure 10a**, we can observe the most

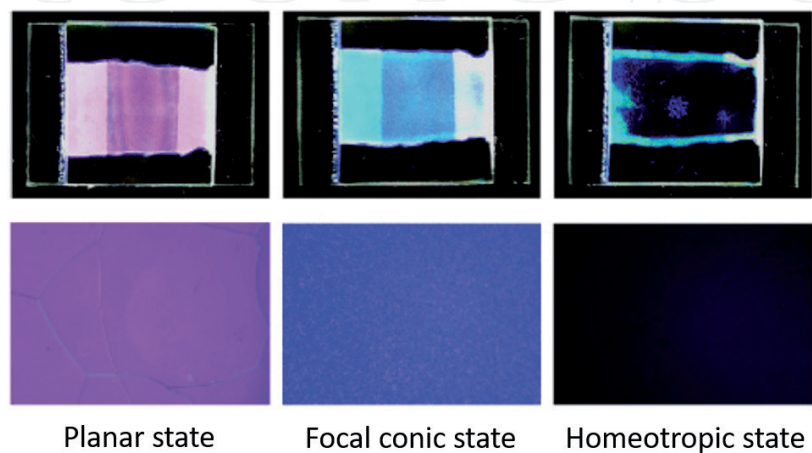


**Figure 9.** Photographs and micrographs of the PC/PSCT device placed between crossed polarizers in P, FC, and H states at zero voltage (adapted from [22–24]).

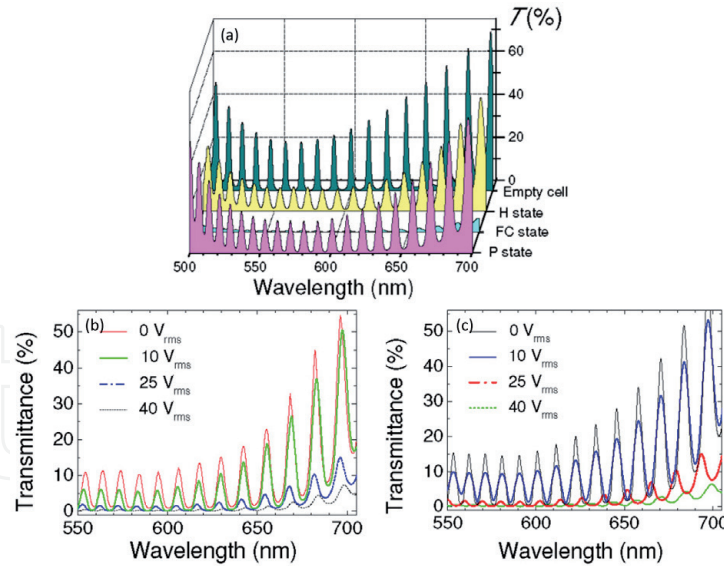


**Figure 10.**

(a) Transmission spectra of the empty PC cell and the PC/PSCT structure in three different states P, FC, and H states. In addition, (b) transmittance of the defect modes from H to FC in the PBG induced by a 100-kHz various voltage amplitudes. (c) Transmittance of the defect modes from P to FC in PC/PSCT induced by various voltage at a fixed frequency of 1 kHz (adapted from [22–24]).

intense defect modes in the empty PC cell because of the transparent air defect. With a PSCT defect layer embedded in the PC device, the PC/PSCT device initially in the H state and the more spectral defect windows in the PBG due to the higher (ordinary) refractive index  $n_o$  in the LC layer. And the FC state is demonstrated when a 30-kHz voltage pulse is applied. The lower transmission of the defect modes in the PBG is also shown in **Figure 10a**. We can employ the defect modes of FC to switch off the PC device by the light scattering property. When the frequency still increases to 100 kHz, the PC/PSCT will be in the P state. The redshifted defect modes is shown and the increasing defect mode number is exhibited (**Figure 10a**). Moreover, **Figure 10b** illustrates the spectra of the PC/PSCT device in the H and FC states induced by various voltage amplitudes at a fixed high frequency of 100 kHz. We can observe that the H state of the cell is the initial state. The intensity strength of the defect modes can be tuned by increasing the voltage. **Figure 10c** demonstrates the transmission spectra of the defect modes by applying various voltage of 0, 10, 25, 40  $V_{rms}$  at a low frequency of 1 kHz. We can easily modulate the strength of defect modes between FC and P states. This powerful photonic device has the potential to expand optics applications, making it use as an electrically tunable device and optically tristable filter based on these special properties.

To conclude, the electrically tunable PC/PSCT devices have been investigated. In addition, the tunability is caused by the incorporation of a PSCT material as a new defect layer in PC structure. This hybrid PC/PSCT owns three stable P, FC, and H states. The electrically tunable PC device has been investigated, and it can be directly switched from one to another stable state by just applying a voltage pulse. Due to the tristability, the optical defect modes of PC/PSCT remain at zero voltages. This PC/PSCT composite device exhibits many different defect mode transmission spectra when we switch among P, FC, and H states. In addition, the intensity of the defect modes can be tuned by the amplitude of voltage as well as the wavelengths can be switched by the frequency in the H and P states. Based on the properties of tristable switching, wavelength controlling, and intensity tunability in the defect modes, the novel PC/PSCT device can be used as a low-power consumption optical filter, light shutter or an electrically intensity modulator without any polarizers, which let the PC/PSCT device more potential for applications.



### 3. Applications in liquid crystal-based photonic crystals

#### 3.1 Electrically switchable liquid crystal-based photonic crystals for a white light laser

Laser source is the most unique light source with many special optical properties such as coherence and collimation. The laser emission needs both the elements: stimulating source and the gain media. Today, various solid and gas materials have been employed as gain media for lasing. However, white light lasers that span the visible spectrum (red, green, and blue colors) are important for lighting, imaging, and communication applications. Recently, the organic white light laser source was successfully demonstrated [32]. Recently, an inorganic semiconductor laser source has also been proposed with a monolithic multi-segment semiconductor nanostructure [33]. Huang et al. also shows that PC/CLC hybrid structure (**Figure 11a**) is a new way to achieve white light laser [34]. In addition, the complex stacking PC/CLC structure is designed (see **Figure 11a**) and can be simply coded as  $[GI(HL)4HH(LH)3]-P(D)P-[(HL)3HH(LH)4IG]$ , where D means the dye-doped CLC (DDCLC); P is the polyimide alignment layer; H and L are the high and low refractive indices of dielectrics; G represents the glass substrate; and I is the ITO. In addition, the high and low refractive indices of dielectric materials are  $Ta_2O_5$  ( $n_H = 2.18$ ) and  $SiO_2$  ( $n_L = 1.47$ ). The configurations of the CLCs in three states (P, FC, and H states) are shown in **Figure 11b**. Note that the voltage  $V_1$  leads to the FC state exhibiting an optical scattering property, and a larger voltage  $V_2$  induces the H state. The transmission spectra of CLC and a PC substrate are also displayed in **Figure 12a**. In addition, the PBG is divided by a defect mode peak at the 640 nm of PBG. The Bragg reflection of DDCLC is located at right half of PBG in hybrid PC cell. The dye composition (C540A, PM580, and LD688) in the PC/DDCLC device was adjusted to fluoresce in three wavelengths (red, green, and blue lasing emissions). However, the artificial defect mode peak in the PC is at 446 nm, which allowed the pumping light to penetrate the PC cell. An organo-inorganic white light laser from PC/DDCLC composed of three colors red, green, and blue lasing emissions is therefore achieved, as displayed in **Figure 12b**. A genuine photo of the PC/DDCLC laser is shown in **Figure 12c**, which is accompanied by the CIE1931 chromaticity diagram. In addition, the color of red, green, and blue are mixed as the discrete

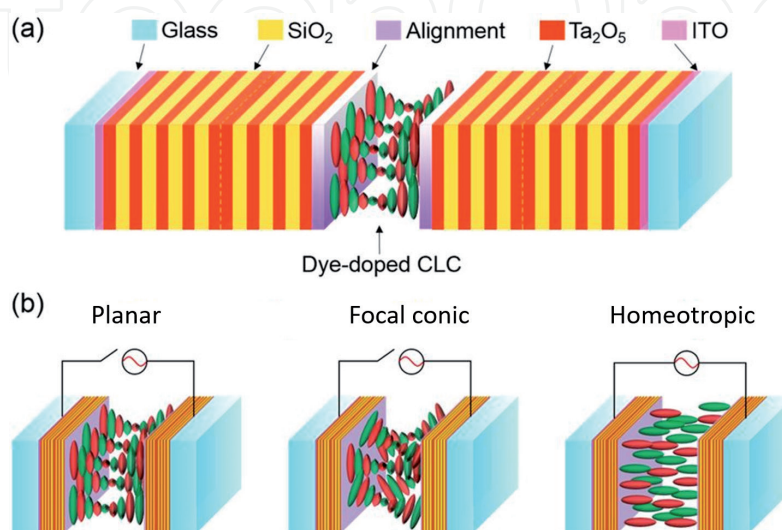


**Figure 11.** Schematics of (a) the hybrid photonic structure and (b) the configurations of the three CLC states in the multilayers device (adapted from [32]).



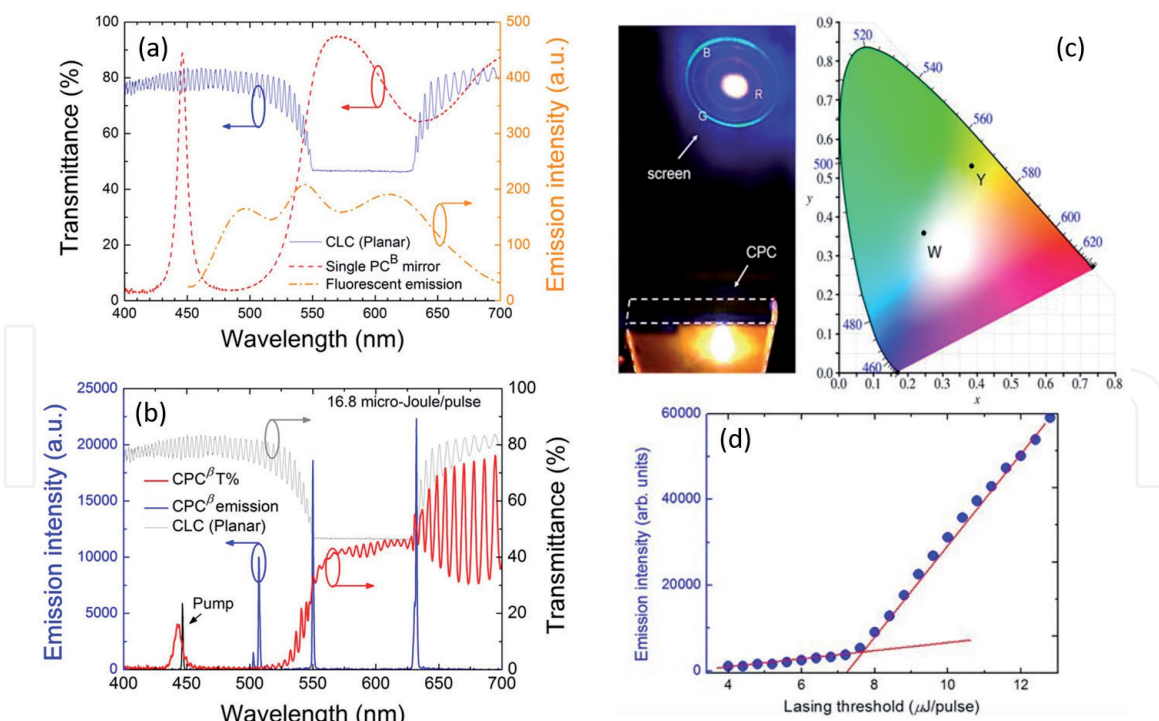


**Figure 12.**

*Spectra of PC/DDCLC. (b) The white-light lasing spectrum and the spectra of PC and the CLC in the planar state. (c) Photograph of a tricolor laser device and the color space coordinates of the PC laser on the CIE 1931 chromaticity diagram. (d) the pumping energy-dependent the lasing emitted from PC/DDCLC device.*

white light laser and depicted in **Figure 12c**. One can tell that the novel PC/DDCLC structure can be really lasing in white light. **Figure 12d** shows the relation between lasing intensity of PC device with the pumping energy. The threshold is about 7.4 μJ/pulse in this PC lasing device.

This is the first demonstration of a discrete white light source (three-colors: red, green, and blue) lasing. The organo-inorganic PC/DDCLC cannot only generate three colors in lasers with a single pump, but also be electrically switched among the three modes lasing. With such properties, lasing wavelength can be altered back and forth in a wavelength range and in a very short response time. In addition, PC/DDCLC lasing device is also cost effective, color tunable, and can be fabricated easily. Moreover, it has been shown that the PC device can be pumped using a simple CW laser. The ability to generate a single-color, two-color, three-color or white-light laser makes a new way to full color display, lighting, and other optics applications. By employing PC/DDCLC lasing device, a small size laser system can be achieved to make the proposed PC/DDCLC applications more feasible and potential.

### 3.2 Liquid crystal-based photonic crystals for pulse compression and signal enhancement in fluorescence applications

Multiphoton fluorescence microscopy, devised in 1990, has become an important technology for bio-applications. The improved axial depth and image penetration depth can reduce the bio-sample damage. This approach demonstrates potential applications in bio-imaging *in vivo* [35]. However, the high intensity of the excitation pulsed laser used in multiphoton fluorescence microscopy inducing the photo-damaging in specimens [36]. In the past, the method to reduce the photo damage in the bio-sample with strengthened multiphoton signal employs the excitation laser with narrower pulse widths. Recently, researchers found that the multiphoton fluorescence can be strengthened with the fluorescence signal, which

is being proportional to the laser pulse widths. In 2001, both scientists McConnell and Riis [37] observed a seven-fold enhancement in two-photon fluorescence by the excitation-compressed laser pulses ( $\sim 35$  fs) [36]. However, by using this laser pulse compression techniques, a dispersion compensator is needed. Thus, the different microscope objectives contribute to different degrees of laser pulse broadening. Recently, Hsiao et al. propose the first PC device enabling on-specimen compression of excited laser pulse. The compression effect occurs after the laser light passing through the objective and photonic components. This will be significant to enhance the multiphoton fluorescence signal. In addition, the PC devices combining with LC materials as defect layer can make the device with the tunable property. From now on, the LC-based PCs for the pulse compression and signal enhancement in multiphoton fluorescence have been proposed.

Moreover, in order to measure the pulse widths through the PC device on-specimen, an optical autocorrelator was employed in the multiphoton fluorescence microscopy. This new approach allows us to detect the autocorrelation signal at the focal plane of the objective, which are shown in **Figure 13a**. In addition, the Ti:sapphire laser is sent through a 50% beam splitter, and one of the optical beams passes through a variable delay line system. Moreover, the multiphoton fluorescence signals can be detected by a photomultiplier tube (PMT). The autocorrelation signal traces with a peak-to-background ratio of the interferences are 8:1 and shown in **Figure 13b** and **c**. We can observe that the envelope of the interferences is fitted to the function of Gaussian. The original pulse width of the commercial Ti-Sapphire laser is about 100 fs. However, the laser pulse width was broadened to be 270 fs after passing through the optical components and objective, (**Figure 13b**). In addition, the laser pulse width decreases in a nonlinear fashion when we increase the power. The most important is the shortest pulse duration is 30 fs (**Figure 13d**). **Figure 14a** shows the images of the red channel at different exposure time under the operating power 40 mW with device and 150 mW without device. If the PC/LC device was not used, the photo damage becomes apparent when the exposure time beyond 1.5 h. If the proposed PC device was

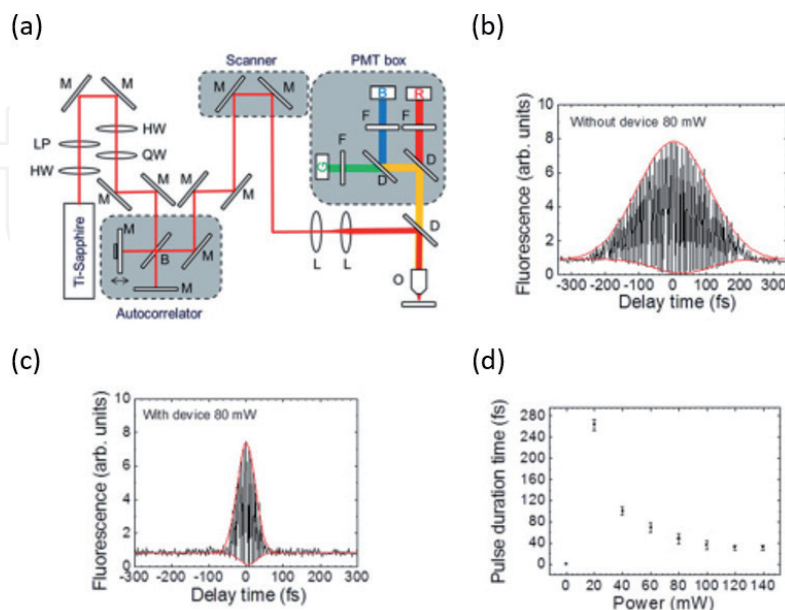


**Figure 13.**  
 (a) The system design of optical autocorrelator in multiphoton fluorescence microscopy. HW is half-wave plates, LP stands for linear polarizers, QW is quarter-wave plates, M means mirrors, B is a beam splitter, L is lenses, O stands for the objective, D means dichroic mirrors, and F stands for filters; (b) and (c) are the autocorrelation traces without and with the PC devices; (d) pulse duration time versus the applied laser powers (adapted from [38]).

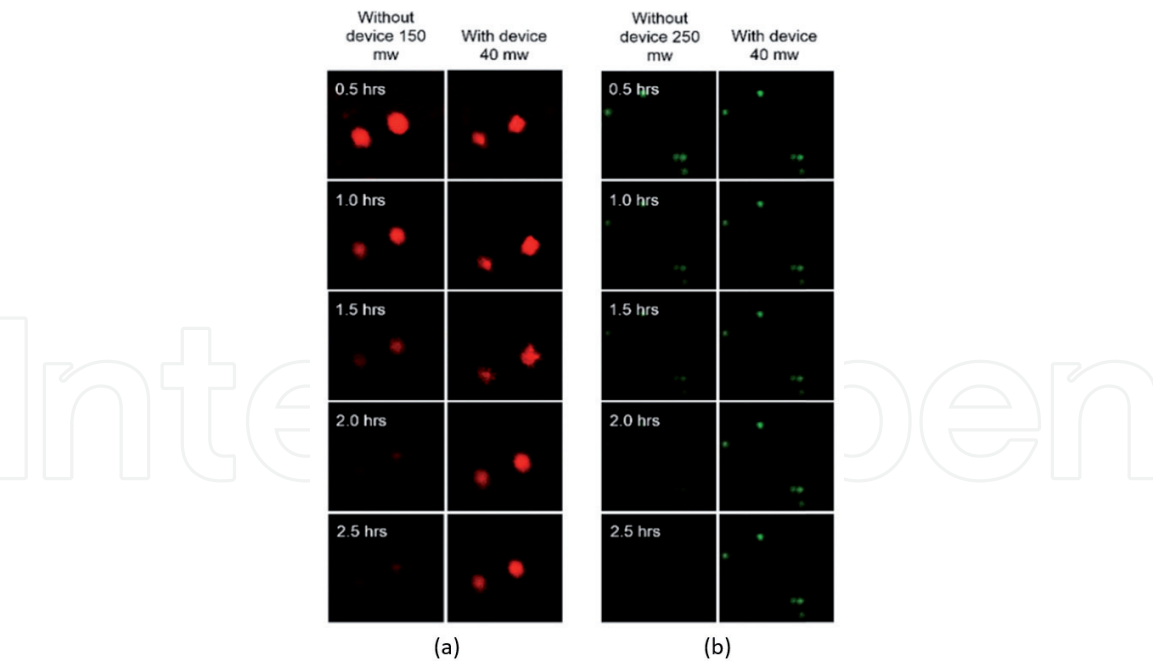


**Figure 14.** The photo images of (a) the red and (b) the green fluorescent balls at different illumination time with and without the PC/LC device (adapted from [38]).

used, the photo damage effect can be easily reduce and lower the excitation power, which is applied to achieve the same signal intensity. We can observe that PC/LC device can efficiently reduce the both operation power and photo damage. In addition, **Figure 14b** shows the same effect of photo damage reducing in the green fluorescent balls under applied voltage 10 V. Thus, this novel PC/LC device is much more powerful for bio-imaging in photo damage reducing. In addition, this PC/LC device for laser pulse compression does not need any dispersion correction, making the biologists easy to use the PC/LC device.

In conclusion, Dr. Hsiao used a PC/LC to compress the laser pulse, exhibiting a 15-fold enhancement of the fluorescence. Without any dispersion compensator, the PC/LC device can be more convenient for nonphotonic researchers. By using the both pulse compression effect of PCs and the tunability of LCs, the PC/LC device shows a new way to enhance the multiphoton fluorescence microscopy with lower photo damage.

### 3.3 Photo-manipulated photonic devices based on tristable chiral-tilted homeotropic nematic liquid crystal

In recent years, energy saving materials have attracted much attention from scientists. The energy saving materials need to own excellent optical stability and do not require constantly applied energy. Based on the stable state natural properties, bistable LC devices are shown and can be used as e-books or e-papers. Recently, compared with the bistable in LC modes, tristable or multi-stable LCs have been scarcely proposed. Historically, the tristable LC mode was first exhibited in a ferroelectric LC system in 1988, and then the first tristable CLC device was later proposed by Hsiao et al. [22–24]. However, the stability of a LC state is very pressure-sensitive of the LCs to be bistable or tristable. Hsiao et al. demonstrate a new tristable optical composite—dye-doped tristable chiral-tilted homeotropic nematic (TCHN). This TCHN mode is extended from the technique of BHN mode. In comparison with BHN, TCHN adopts a common nematic LC material instead of DFLC material; it possesses an additional stable state and is stress-insensitive in



stable states. Recently, Huang et al. proposed the spectral properties of an optically switchable TCHN incorporated as a tunable defect layer in PC structure. By controlling the polarization angle of the incident light as well as the intensity ratio between UV and green light, the tunable transmission characteristics of defect modes in the PC/TCHN were obtained. The hybrid PC structure realizes photo-tunability of defect mode peaks within the photonic bandgap. The PC/TCHN has much potential for many photonic applications such as a low-power consumption filter and an optically controllable intensity modulator device.

A schematic of the hybrid PC/TCHN structure is shown in **Figure 15a**. The optical switching of TCHN is among the tT, fingerprint (FP), and tH states as the new tristable PC device and is displayed in **Figure 15b**. The chiral bis(azobenzene) molecule is photoresponsive and is used in TCHN system. The chiral has two azo linkages to confer two distinct isomeric conformations: the rod like *trans* form and the bent *cis* form. The photo-induced unwinding effect caused by the *trans*-to-*cis* isomerization exposed to UV light and the winding effect due to the *cis*-to-*trans* isomerization under green light illumination. Based on the mechanism, we can optically switch TCHN among the tT, FP, and tH states. The experimental spectra of the PC/TCHN devices were measured under irradiation by controlling both green light and UV light. In Hsiao's paper, the used green light is from LED at wavelength of 524 nm and the UV light is from a UV LED at wavelength of 365 nm. Based on the two mixed irradiation lights, the PC/TCHN can be switched among three stable states (tT, FP, and tH). In addition, **Figure 15** shows the micrographic optical textures of the state-transform process among tristable tT, FP, and tH states under a crossed-polarizing microscope. Moreover, **Figure 15a, c, and e** shows the micrographic optical textures of tT, FP, and tH states, respectively. The tH state is completely dark state in the crossed-polarizer scheme because of no birefringence effect. The tT state is a bright optical texture with some rubbing traces, and the FP texture involves the lying helix structure of chiral nematic molecules as shown. The transmission spectra of defect modes within the PBG at various irradiations are also proposed. **Figure 16** demonstrates the transmittance spectra of defect modes that are controlled by the UV light with various intensities. In addition, the intensity of green light is fixed at  $2.02 \text{ mW/cm}^2$ . From **Figure 16f**, we can observe that the PC/TCHN device is exhibited in the tT state when intensity of UV is  $0 \text{ mW/cm}^2$  because of the azo chiral dopant being in the *trans*-form. However, the *cis*-form dopant molecules will increase when intensity of UV is strengthened gradually. Because the high-pretilt angle of LC and particular d/p conditions,

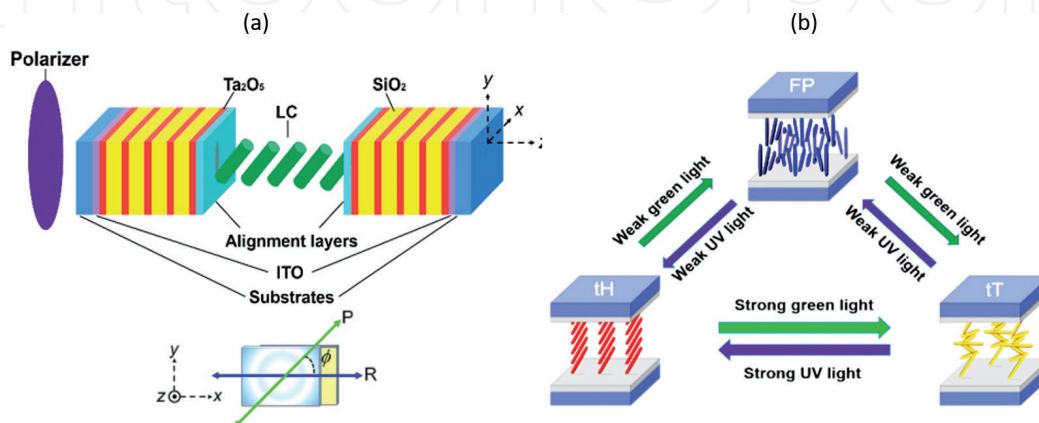


**Figure 15.**  
 (a) Sandwich structure of the PC/TCHN device. The arrows in the device's front view show the transmission axis of the polarizer (P) and rubbing direction (R). (b) Operating mechanisms of photo-induced TCHN switching among the tH, FP and tT states (adapted from [34]).



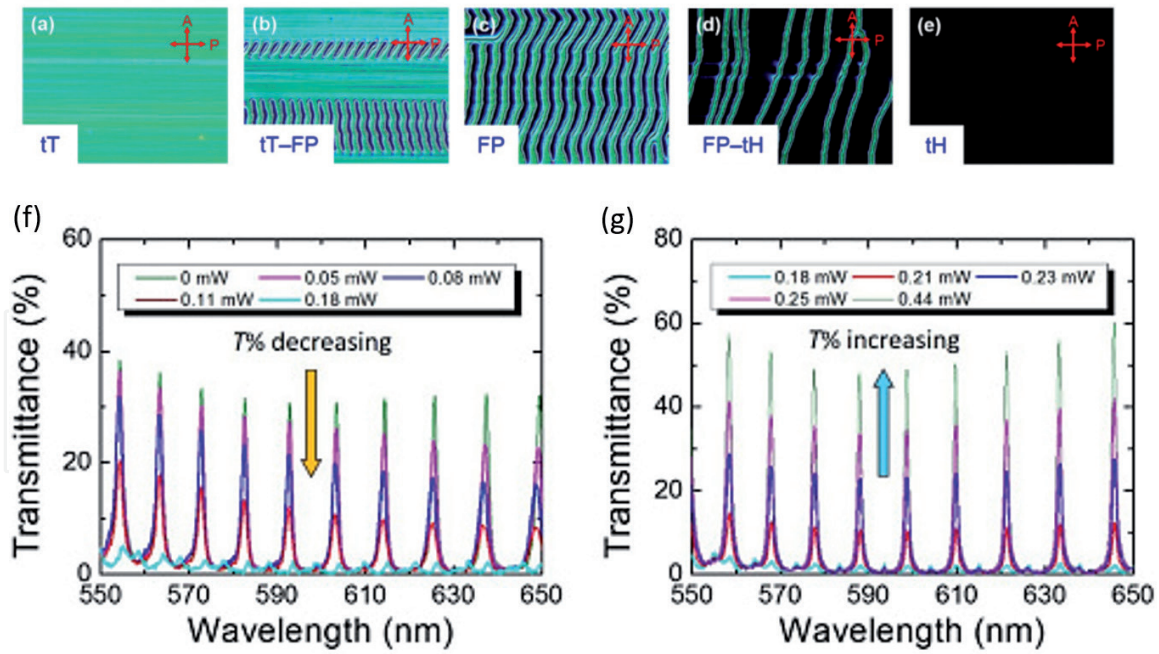


**Figure 16.** The transition process among three stable states by increasing irradiation ratios between UV and green light. (a) The tT state; (b) the coexistence of tT and FP states; (c) the FP state; (d) the coexistence of FP and tH states; (e) the pure tH state of a TCHN. The arrows indicate the transmission axes of the polarizer (P) and analyzer (A). In addition, photo-manipulated transmittance of the defect modes under irradiation by various UV powers. (f) From the tT to the FP state and (g) from the FP to tH state (adapted from [34]).

the FP texture will appear. Then, we can see that the intensities of defect mode vanish because of strong scattering. However, the defect mode shifts to distinct wavelengths and emerges again with enhanced intensity of UV. When the azo chiral molecules become fully converted to the trans-form at  $0.44 \text{ mW/cm}^2$ , the PC/TCHN comes to the tH state and the transmittance of defect modes reaches the highest intensity as shown in **Figure 16g**. Based on these optical properties, the PC/TCHN device can be used as tunable optical filters.

In conclusion, a novel concept of photo-switchable PC/TCHN devices is proposed. In comparison with its bistable counterpart BHN, the TCHN can be prepared using a regular nematic host LC material (e.g., E7 in experimental from Huang et al.). The PC/TCHN device owns optical tristability and tunability in wavelength and intensities of the defect modes by photo manipulating. By adjusting the ratio of the UV and green light intensity, the defect modes of PC/TCHN not only show a variation in spectral amplitude through the stable FP state, but also can control the wavelengths between the stable tT and tH states. This novel PC/TCHN mode and the special properties of TCHN material should be fully developed for next potential photonic applications [39–72].

## 4. Conclusions

In this chapter, PC/NLC and PC/chiral LC devices, which exhibit special photonic applications and several fascinating features have been reviewed. In addition, the optical properties of defect modes of PC switching among each state are reported. In Section 2.1, “Photonic crystals with a nonchiral nematic liquid crystal,” the mechanism of defect modes in nonchiral PC is well-described by OPL. The shifting can be understood from a change in  $n_{\text{eff}}$  under applied voltage. Section 2.2 “Chiral-tilted homeotropic nematic liquid crystal-based

photonic crystal devices,” propose the new type of chiral nematic LC (BHN) in PC device. The optical properties and switching mechanism of four tH, bH, bT, and tT states of the PC/BHN device are proposed. In addition, Section 2.3 “Chiral nematic and cholesteric liquid crystal with photonic crystal devices,” and Section 2.4 “Tristable photonic-crystal devices with polymer-stabilized cholesteric textures.” are the typical chiral nematic or CLC structure within PC devices. The three states of P, FC, and H states from CLCs are used for defect modes controlling in PCs. Thus, the configuration of many types of PC/CLC cell applications, including the design of PC multilayers for applications is schematically depicted. I introduce the three PC applications; Session 3.1 introduces “Electrically switchable liquid crystal-based photonic crystals for a white-light laser.” The first PC/LC white light laser is invented, and the mechanism of the laser chip is shown. Session 3.2 shows “Liquid crystal-based photonic crystals for pulse compression and signal enhancement in fluorescence applications,” and it is the first PC/LC device to achieve the pulse compression. From now on, the PC/LC can be as fluorescence enhancement applications. Session 3.3 demonstrates “Photo-manipulated photonic devices based on tristable chiral-tilted homeotropic nematic liquid crystal.” In addition to this, many PC/LC applications, such as optical devices, tunable optical filters, tunable optical modulators, and so on, are also developed in recent year. In conclusion, PC/LC devices are new tools to understand and modulate light. It holds good potential to become a useful tool in our daily life.

## Acknowledgements


This work was financially supported by the Ministry of Science and Technology, Taiwan, under grant No. 107-2218-E-038-007-MY, and Taipei Medical University, Taiwan, under grant No. TMU106-AE1-B49.

## Author details

Yu-Cheng Hsiao  
Graduate Institute of Biomedical Optomechatronics, College of Biomedical Engineering, Taipei Medical University, Taipei, Taiwan

\*Address all correspondence to: [ychsiao@tmu.edu.tw](mailto:ychsiao@tmu.edu.tw)

## IntechOpen

© 2019 The Author(s). Licensee IntechOpen. This chapter is distributed under the terms of the Creative Commons Attribution License (<http://creativecommons.org/licenses/by/3.0>), which permits unrestricted use, distribution, and reproduction in any medium, provided the original work is properly cited. 

## References

- [1] John S. Strong localization of photons in certain disordered dielectric superlattices. *Physical Review Letters*. 1987;**58**(23):2486-2489
- [2] Yablonovitch E. Inhibited spontaneous emission in solid-state physics and electronics. *Physical Review Letters*. 1987;**58**(20):2059-2062
- [3] Fleming JG, Lin S-Y. Three-dimensional photonic crystal with a stop band from 1.35 to 1.95  $\mu\text{m}$ . *Optics Express*. 1999;**24**(1):49-51
- [4] Imada M, Noda S, Chutinan A, Tokuda T, Murata M, Sasaki G. Coherent two-dimensional lasing action in surface-emitting laser with triangular-lattice photonic crystal structure. *Applied Physics Letters*. 1999;**75**(3):316-318
- [5] Knight JC. Photonic crystal fibres. *Nature*. 2003;**424**(6950):2486-2589
- [6] Nelson BE, Gerken M, Miller DAB, Piestun R, Lin C-C, Harris JS. Use of a dielectric stack as a one-dimensional photonic crystal for wavelength demultiplexing by beam shifting. *Optics Express*. 2000;**25**(20):1502-1504
- [7] Park SH, Xia B, Gates Y. A three-dimensional photonic crystal operating in the visible region. *Advanced Materials*. 1999;**11**(6):462-466
- [8] Painter O, Lee RK, Scherer AY, O'Brien JDA, Dapkus PD, Kim I. Two-dimensional photonic band-gap defect mode laser. *Science*. 1999;**284**(5421):1819-1821
- [9] Knight JC, Broeng J, Birks TA, Russell PSJ. Photonic band gap guidance in optical fibers. *Science*. 1998;**282**(5393):1476-1478
- [10] Blanco A, Chomski E, Grabtchak S, Ibisate M, John S, Leonard SW, et al. Large-scale synthesis of a silicon photonic crystal with a complete three-dimensional bandgap near 1.5 micrometers. *Nature*. 2000;**405**(6785):437-440
- [11] Chow E, Lin SY, Johnson SG, Villeneuve PR, Joannopoulos JD, Wendt JR, et al. Three-dimensional control of light in a two-dimensional photonic crystal slab. *Nature*. 2000;**407**(6807):983-986
- [12] Ozaki R, Matsui T, Ozaki M, Yoshino K. Electro-tunable defect mode in one-dimensional periodic structure containing nematic liquid crystal as a defect layer. *Japanese Journal of Applied Physics*. 2002;**41**(12B):L1482-L1484
- [13] Matsuhisa Y, Ozaki R, Takao Y, Ozaki M. Linearly polarized lasing in one dimensional hybrid photonic crystal containing cholesteric liquid crystal. *Journal of Applied Physics*. 2007;**101**(3):033120
- [14] Matsuhisa Y, Ozaki R, Yoshino K, Ozaki M. High Q defect mode and laser action in one-dimensional hybrid photonic crystal containing cholesteric liquid crystal. *Applied Physics Letters*. 2006;**89**(10):101109
- [15] Ozaki R, Matsuhisa Y, Ozaki M, Yoshino K. Low driving voltage tunable laser based on one-dimensional photonic crystal containing liquid crystal defect layer. *Molecular Crystals and Liquid Crystals*. 2005;**441**(1):87-95
- [16] Ozaki R, Ozaki M, Yoshino K. Defect mode switching in one-dimensional photonic crystal with nematic liquid crystal as defect layer. *Japanese Journal of Applied Physics*. 2003;**42**(6B):L669-L671
- [17] Park B, Kim M, Kim SW, Kim IT. Circularly polarized unidirectional



lasing from a cholesteric liquid crystal layer on a 1-D photonic crystal substrate. *Optics Express*. 2009;**17**(15):12323-12331

[18] Arkhipkin VG, Gunyakov VA, Myslivets SA, Zyryanov VY, Shabanov VF. Angular tuning of defect modes spectrum in the one-dimensional photonic crystal with liquid-crystal layer. *European Physical Journal E*. 2007;**24**(3):297-302

[19] Arkhipkin VG, Gunyakov VA, Myslivets SA, Gerasimov VP, Zyryanov VY, Vetrov SY, et al. One-dimensional photonic crystals with a planar oriented nematic layer: Temperature and angular dependence of the spectra of defect modes. *Journal of Experimental and Theoretical Physics*. 2008;**106**(2):388-398

[20] Zyryanov VY, Gunyakov VA, Myslivets SA, Arkhipkin VG, Shabanov VF. Electrooptical switching in a one-dimensional photonic crystal. *Molecular Crystals and Liquid Crystals*. 2008;**488**(1):118-126

[21] Zyryanov VY, Myslivets SA, Gunyakov VA, Parshin AM, Arkhipkin VG, Shabanov VF, et al. Magnetic-field tunable defect modes in a photonic-crystal/liquid-crystal cell. *Optics Express*. 2010;**18**(2):1283-1288

[22] Hsiao Y-C, Hou C-T, Zyryanov VY, Lee W. Multichannel photonic devices based on tristable polymer-stabilized cholesteric textures. *Optics Express*. 2011;**19**(8):7349-7355

[23] Hsiao Y-C, Tang C-Y, Lee W. Fast-switching bistable cholesteric intensity modulator. *Optics Express*. 2011;**19**(10):9744-9749

[24] Hsiao Y-C, Wu C-Y, Chen C-H, Zyryanov VY, Lee W. Electro-optical device based on photonic structure with a dual-frequency cholesteric

liquid crystal. *Optics Letters*. 2011;**36**(14):2632-2634

[25] Wang CT, Chen CW, Yang TH, Nys I, Li CC, Lin TH, et al. Electrically assisted bandedge mode selection of photonic crystal lasing in chiral nematic liquid crystals. *Applied Physics Letters*. 2018;**112**(4):043301

[26] Ye L, Wang Y, Feng Y, Liu B, Gu B, Cui Y, et al. Thermally switchable photonic band-edge to random laser emission in dye-doped cholesteric liquid crystals. *Laser Physics Letters*. 2018;**15**(3):035002

[27] Ozaki R, Ozaki M, Yoshino K. Defect mode in one-dimensional photonic crystal with in-plane switchable nematic liquid crystal defect layer. *Japanese Journal of Applied Physics*. 2004;**43**(11B):L1477-L1479

[28] Lin Y-T, Chang W-Y, Wu C-Y, Zyryanov VY, Lee W. Optical properties of one-dimensional photonic crystal with a twisted-nematic defect layer. *Optics Express*. 2010;**18**(26):26959-26964

[29] Gooch CH, Tarry HA. The optical properties of twisted nematic liquid crystal structures with twist angles < 90 degrees. *Journal of Physics D: Applied Physics*. 1975;**8**(13):1575-1584

[30] Hsiao YC, Zou YH, Timofeev IV, Zyryanov VY, Lee W. Spectral modulation of a bistable liquid-crystal photonic structure by the polarization effect. *Optical Materials Express*. 2013;**3**(6):821-828

[31] Ma J, Shi L, Yang D-K. Bistable polymer stabilized cholesteric texture light shutter. *Applied Physics Express*. 2010;**3**(2):021702

[32] Ha NY et al. Simultaneous red, green, and blue lasing emissions in a single pitched cholesteric liquid



crystal system. *Advanced Materials*. 2008;**20**:2503-2507

[33] Fan F, Turkdogan S, Liu Z, Shelhammer D, Ning CZ. A monolithic white laser. *Nature Nanotechnology*. 2015;**10**:796-803

[34] Huang KC, Hsiao YC, Timofeev IV, Zyryanov VY, Lee W. Photo-manipulated photonic bandgap devices based on optically tristable chiral-tilted homeotropic nematic liquid crystal. *Optics Express*. 2016;**24**(22):25019-25025

[35] Helmchen F, Denk W. Deep tissue two-photon microscopy. *Nature Methods*. 2005;**2**(12):932-940

[36] Hopt A, Neher E. Highly nonlinear photodamage in two-photon fluorescence microscopy. *Biophysical Journal*. 2001;**80**(4):2029-2036

[37] McConnell G, Riis E. Two-photon laser scanning fluorescence microscopy using photonic crystal fiber. *Journal of Biomedical Optics*. 2004;**9**(5):922-928

[38] Hsiao YC. Liquid crystal-based tunable photonic crystals for pulse compression and signal enhancement in multiphoton fluorescence. *Optical Materials Express*. 2016;**6**(6):1929-1934

[39] Bao R, Liu C-M, Yang D-K. Smart bistable polymer stabilized cholesteric texture light shutter. *Applied Physics Express*. 2009;**2**:112401

[40] Berreman DW, Heffner WR. New bistable cholesteric liquid-crystal display. *Applied Physics Letters*. 1980;**37**(1):109-111

[41] Bobrovsky AY, Boiko NI, Shibaev VP, Wendorff JH. Cholesteric mixtures with photochemically tunable circularly polarized fluorescence. *Advanced Materials*. 2003;**15**(4):282-287

[42] Choi SS, Morris SM, Huck WTS, Coles HJ. Electrically tuneable liquid crystal photonic bandgaps. *Advanced Materials*. 2009;**21**(38):3915-3918

[43] Hsiao YC, Wang HT, Lee W. Thermoelectric generation of defect modes in a photonic liquid crystal. *Optics Express*. 2014;**22**(3):3593-3599

[44] Hsiao YC, Lee W. Lower operation voltage in dual-frequency cholesteric liquid crystals based on the thermoelectric effect. *Optics Express*. 2013;**21**(20):23927-23933

[45] Hsiao YC, Sung YC, Lee MJ, Lee W. Highly sensitive color-indicating and quantitative biosensor based on cholesteric liquid crystal. *Biomedical Optics Express*. 2015;**6**(12):5033-5038

[46] Hsiao YC, Timofeev IV, Zyryanov VY, Lee W. Hybrid anchoring for a color-reflective dual-frequency cholesteric liquid crystal device switched by low voltages. *Optical Materials Express*. 2015;**5**(11):2715-2720

[47] Hsiao YC, Huang KC, Lee W. Photo-switchable chiral liquid crystal with optical tristability enabled by a photoresponsive azo-chiral dopant. *Optics Express*. 2017;**25**(3):2687-2693

[48] Hsiao YC, Lee W. Polymer stabilization of electrohydrodynamic instability in non-iridescent cholesteric thin films. *Optics Express*. 2015;**23**(17):22636-22642

[49] Hsiao YC, Yang ZH, Shen D, Lee W. Red, green, and blue reflections enabled in an electrically tunable helical superstructure. *Advanced Optical Materials*. 2018;**6**(5):1701128

[50] Hsu J-S. Stability of bistable chiral-tilted homeotropic nematic liquid crystal displays. *Japanese Journal of Applied Physics*. 2007;**46**(11):7378-7381

- [51] Hsu J-S, Liang B-J, Chen S-H. Bistable chiral tilted-homeotropic nematic liquid crystal cells. *Applied Physics Letters*. 2004;**85**(23):5511-5513
- [52] Hsu J-S, Liang B-J, Chen S-H. Dynamic behaviors of dual frequency liquid crystals in bistable chiral tilted-homeotropic nematic liquid crystal cell. *Applied Physics Letters*. 2007;**89**(5):091520
- [53] Huang CY, Fu K-Y, Lo K-Y, Tsai M-S. Bistable transfective cholesteric light shutters. *Optics Express*. 2003;**11**(6):560-565
- [54] Huang Y, Zhou Y, Doyle C, Wu S-T. Tuning the photonic band gap in cholesteric liquid crystals by temperature-dependent dopant solubility. *Optics Express*. 2006;**14**(3):1236-1244
- [55] Jhun CG, Chen CP, Lee UJ, Lee SR, Yoon TH, Kim JC. Tristable liquid crystal display with memory and dynamic operating modes. *Applied Physics Letters*. 2006;**89**(12):123507
- [56] Kasano M, Ozaki M, Yoshino K, Ganzke D, Haase W. Electrically tunable waveguide laser based on ferroelectric liquid crystal. *Applied Physics Letters*. 2003;**82**(23):4026-4028
- [57] Krauss TF, La Rue D, Richard M, Brand S. Two-dimensional photonic bandgap structures operating at near-infrared wavelengths. *Nature*. 1996;**383**(6602):699-702
- [58] Miroshnichenko AE, Brasselet E, Kivshar YS. All-optical switching and multistability in photonic structures with liquid crystal defects. *Applied Physics Letters*. 2008;**92**(25):253306
- [59] Miroshnichenko AE, Brasselet E, Kivshar YS. Light-induced orientational effects in periodic photonic structures with pure and dye-doped nematic liquid crystal defects. *Physical Review A*. 2008;**78**(5):053823
- [60] Morris SM, Ford AD, Pivnenko MN, Coles HJ. Enhanced emission from liquid-crystal lasers. *Journal of Applied Physics*. 2005;**97**(2):023103
- [61] Ozaki R, Moritake H, Yoshino K, Ozaki M. Analysis of defect mode switching response in one-dimensional photonic crystal with a nematic liquid crystal defect layer. *Journal of Applied Physics*. 2007;**101**(3):033503
- [62] Timofeev IV, Lin Y-T, Gunyakov VA, Myslivets SA, Arkhipkin VG, Ya VS, et al. Voltage-induced defect mode coupling in a one-dimensional photonic crystal with a twisted-nematic defect layer. *Physical Review E*. 2012;**85**(1):011705
- [63] Wen C-H, Wu S-T. Dielectric heating effects of dual-frequency liquid crystals. *Applied Physics Letters*. 2005;**86**(23):231104
- [64] Wu S-T, Wu C-S. Mixed-mode twisted nematic liquid crystal cells for reflective displays. *Applied Physics Letters*. 1996;**68**(11):1455-1457
- [65] Wu C-Y, Zou Y-H, Timofeev I, Lin Y-T, Zyryanov VY, Hsu J-S, et al. Tunable bi-functional photonic device based on one-dimensional photonic crystal infiltrated with a bistable liquid-crystal layer. *Optics Express*. 2011;**19**(8):7349-7355
- [66] Xu M, Yang D-K. Dual frequency cholesteric light shutters. *Applied Physics Letters*. 1997;**70**(6):720-722
- [67] Yao I-A, Yang C-L, Chen C-J, Pang J-P, Liao S-F, Li J-H, et al. Bistability of splay and  $\pi$ -twist states in a chiral-doped dual frequency liquid crystal cell. *Applied Physics Letters*. 2009;**94**(7):071104

[68] Yeh PH, Gu C. Normal modes of propagation in a general TN-LC. In: Optics of Liquid Crystal Display. Canada: John Wiley & Sons. ISBN 0-471-18201-X; 1999. pp. 130-136

[69] Yeh PH, Gu C. Light propagation in uniaxial media. In: Optics of Liquid Crystal Display. Canada: John Wiley & Sons. ISBN 0-471-18201-X; 1999. pp. 63-68

[70] Yeung Fion S-Y, Xie F-C, Wan Jones T-K, Lee FK, Tsui Ophelia KC, Sheng P, et al. Liquid crystal pretilt angle control using nanotextured surfaces. Journal of Applied Physics. 2006;**99**(12):124506

[71] Yin Y, Shiyanovskii SV, Lavrentovich OD. Electric heating effects in nematic liquid crystals. Journal of Applied Physics. 2006;**100**(2):024906

[72] Yokoyama S, Mashiko S, Kikuchi H, Uchida K, Nagamura T. Laser emission from a polymer-stabilized liquid-crystalline blue phase. Advanced Materials. 2006;**18**(1):48-51